

Flow structures in zero pressure-gradient turbulent boundary layers.

By Jens M. Österlund, Björn Lindgren & Arne V. Johansson

Dept. of Mechanics, KTH, SE-100 44 Stockholm, Sweden

To be submitted

An experimental investigation on flow structures was performed in a high Reynolds number zero pressure-gradient turbulent boundary layer. Results are presented for the fluctuating wall-shear stress obtained simultaneously at two spanwise positions using a micro-machined hot-film sensor. Two-point correlations are presented and the mean streak spacing is evaluated from the two-point correlation of high-pass filtered wall-shear-stress signals. The streak spacing was found to be approximately $110\nu/u_\tau$ at the Reynolds number $Re_\theta = 9700$.

Experiments involving the simultaneous measurement of the wall-shear stress and the streamwise velocity component in an array of points in the streamwise-wall normal (x, y) -plane, directly above the hot-film, was also conducted. Results are presented for the conditionally averaged velocity field obtained by detecting turbulence generating events from the wall-shear stress, and two-point correlation measurements between the wall-shear stress and the streamwise velocity. Local propagation velocities and details of shear-layer structures are presented.

The scaling of the occurrence of VITA events in the buffer layer was investigated and a mixed time scale (*i.e.* the geometric mean of the inner and outer timescale) was found to give a satisfactory collapse of the data.

1. Introduction

The statistical, Reynolds averaged, description of turbulent boundary layers hides a wealth of structure-related phenomena and a quite intermittent character of *e.g.* turbulence production. This has been illustrated in flow visualizations, measurements and from DNS-generated data in a large number of papers, see *e.g.* the landmark paper of Kline *et al.* (1967), who showed that a significant part of the turbulence could be described in terms of deterministic events. These studies showed that in the close proximity of the wall the flow is characterized by elongated regions of low and high speed fluid of fairly regular spanwise spacing of about $\lambda^+ = 100$. Sequences of ordered motion occur randomly in space and time where the low-speed streaks begin to oscillate and to

suddenly break-up into a violent motion, a “burst”. Kim *et al.* (1971) showed that the intermittent bursting process is closely related to shear-layer like flow structures in the buffer region, and also that roughly 70% of the total turbulence production was associated with the bursting process. The “bursts” were further investigated by Corino & Brodkey (1969) and it was found that two kinds of turbulence producing events are present. The ejection: involving rapid outflow of low speed fluid from the wall and sweeps: large scale motions originating in the outer region flowing down to the wall. Smith & Metzler (1983) investigated the characteristics of low-speed streaks using hydrogen bubble-flow and a high-speed video system. They found that the streak spacing increased with the distance from the wall. Furthermore, they found that the persistence of the streaks was one order of magnitude longer than the observed bursting times associated with the wall region turbulence production.

To obtain quantitative data to describe the structures a reliable method to identify bursts with velocity or wall-shear stress measurements is needed. Conditional averaging using some triggering signal can be used to study individual events such as bursts or ejections and was first employed by Kovaszny *et al.* (1970). The triggering signal must be intermittent and closely associated with the event under study. Wallace *et al.* (1972) and Willmart & Lu (1972) introduced the uv quadrant splitting scheme. Blackwelder & Kaplan (1976) developed the VITA technique to form a localized measure of the turbulent kinetic energy and used it to detect shear-layer events. The detected events were studied using conditional averaging. Chen & Blackwelder (1978) added a slope condition to the VITA technique to detect only events corresponding to rapid acceleration. The behavior of the conditionally averaged streamwise velocity detected on strong accelerating events may be explained by tilted shear-layers that are convected past the sensor. Kreplin & Eckelmann (1979) measured the angle of the shear-layer front from the wall and found that nearest to the wall it was about 5° . At larger distances from the wall Head & Bandyopadhyay (1981) found the angle to be much steeper, about 45° . Gupta *et al.* (1971) investigated the spatial structure in the viscous sub-layer using an array of hot-wires distributed in the spanwise direction. They used a VITA correlation technique to determine the spanwise separations between streaks in the viscous-sub layer. The evolution of shear layers was studied by Johansson *et al.* (1987a) in the Göttingen oil channel by use of two-probe measurements in the buffer region of the turbulent channel flow. The bursting frequency in turbulent boundary layers was first investigated by Rao *et al.* (1971), their experiments indicated that outer scaling gave the best collapse of the data. Later, Blackwelder & Haritonidis (1983) carried out experiments on the bursting frequency in turbulent boundary layers. They found the non-dimensional bursting frequency was independent of Reynolds number when scaled with the inner time scale and found a strong effect of spatial averaging for sensors larger than 20 viscous

length scales. Alfredsson & Johansson (1984) studied the frequency of occurrence for bursts in turbulent channel flow, where they found the governing time scale to be a mixture (the geometric mean) of the inner and outer time scales. Johansson *et al.* (1991) analyzed near-wall flow structures obtained from direct numerical simulation of channel flow (Kim *et al.* 1987) using conditional sampling techniques. They also analyzed the space-time evolution of structures and asymmetry in the spanwise direction was found to be an important characteristic of near-wall structures, and for shear-layers in particular.

There seems to be no consensus on how to define a coherent structure and several definitions exist. In a review article on the subject Robinson (1991) defines a coherent structure as

... a three-dimensional region of the flow over which at least one fundamental flow variable (velocity component, density, temperature, etc.) exhibits significant correlation with itself or with another variable over a range of space and/or time that is significantly larger than the smallest local scales of the flow.

Other more restricted definitions are given by *e.g.* Hussain (1986) and Fiedler (1986). Here we will deal mainly with the streaks found in the viscous sub-layer and the connected shear-layer type structures that are believed to be major contributors to the turbulence generation.

The majority of the experimental studies on structures in turbulent boundary layers have been conducted at low Reynolds numbers ($Re_\theta < 5000$), where flow visualization and high resolution velocity measurements are relatively easy to obtain. One of the objectives with this study was therefore to extend the knowledge about turbulence structures to high Reynolds numbers.

Three types of investigations were carried out. First, we investigate the mean streak spacing by measurements of the instantaneous wall-shear stress in two points with different spanwise separations. Secondly, the scaling of the “bursting frequency” was investigated by detection of the frequency of VITA events in the buffer region. Thirdly, a single wire probe was traversed in a streamwise wall-normal (x, y) -plane above the hot-film sensor, with the aim to detect and characterize shear-layer type events and to determine their local propagation velocity.

2. Experimental facility

The flow field of a zero pressure-gradient turbulent boundary layer was established on a seven meter long flat plate mounted in the test section of the MTL wind-tunnel at KTH. The MTL wind tunnel is of closed-return type designed with low disturbance level as the primary design goal. A brief description of the experimental set-up is given below. A more detailed description of the boundary layer experimental set-up can be found in paper 7.

After the test section the flow passes through diffusers and two 90° turns before the fan. A large fraction of the wind-tunnel return circuit is equipped with noise-absorbing walls to reduce acoustic noise. The flow quality of the MTL wind-tunnel was reported by Johansson (1992). For instance, the streamwise turbulence intensity was found to be less than 0.02%. The air temperature can be controlled to within $\pm 0.05^\circ\text{C}$, which is very important for this study since the primary measurement technique was hot-wire/hot-film anemometry, where a constant air temperature during the measurement is a key issue. The test section has a cross sectional area of $0.8\text{ m} \times 1.2\text{ m}$ (height \times width) and is 7 m long. The upper and lower walls of the test section can be moved to adjust the pressure distribution. The maximum variation in mean velocity distribution along the boundary layer plate was $\pm 0.15\%$.

The plate is a sandwich construction of aluminum sheet metal and square tubes in seven sections plus one flap and one nose part, with the dimensions 1.2 m wide and 7 m long excluding the flap. The flap is 1.5 m long and is mounted in the following diffuser. This arrangement makes it possible to use the first 5.5 m of the plate for the experiment. One of the plate sections was equipped with two circular inserts, one for a plexiglas plug where the measurements were done, and one for the traversing system. The traversing system was fixed to the plate to minimize any vibrations and possible deflections. The distance to the wall from the probe was determined by a high magnification microscope. The absolute error in the determination of the wall distance was within $\pm 5\mu\text{m}$.

The boundary layer was tripped at the beginning of the plate and the two-dimensionality of the boundary layer was checked by measuring the spanwise variation of the wall shear stress τ_w . The maximum spanwise variation in friction velocity $u_\tau = \sqrt{\tau_w/\rho}$ was found to be less than $\pm 0.7\%$.

The ambient conditions were monitored by the measurement computer during the experiments using an electronic barometer and thermometer (FCO 510 from Furness Ltd., UK). The reference conditions used in the calibration of the probes were determined using a Prandtl tube in the free-stream directly above the measurement station. The pressure and temperature were monitored at all times during the experiments using a differential pressure transducer and a thermometer connected directly to the measurement computer. The accuracy of the pressure measurement was 0.25 % and the accuracy of the temperature measurement was 0.02°C .

Constant temperature hot-wire anemometry was used in all velocity measurements. All hot-wire probes were designed and built at the lab. Three sizes of single-wire probes were used in the experiments with wire diameters of: 2.5, 1.27 and $0.63\mu\text{m}$ and a length to diameter ratio always larger than 200.

The MEMS hot-film (figure 1) used in the wall-shear stress measurements was designed by the MEMS group at UCLA/Caltec (Jiang *et al.* 1996, 1997; Ho & Tai 1998). It was flush-mounted with a printed circuit board for electrical

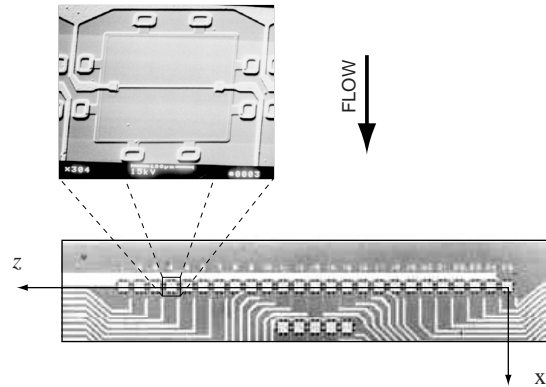


FIGURE 1. Enlargement of the MEMS hot-film sensor chip from UCLA/Caltech (Jiang *et al.* 1996) showing the array of 25 sensors used, seen as the row of white squares on the z -axis. A blow-up of one of the hot-films is also shown.

connections which in turn was flush-mounted into a Plexiglas plug fitting into the instrumentation insert of the measurement plate-section. Accurate alignment of the chip surface and the circuit board and the flat plate was achieved using a microscope during the mounting of the sensor set-up. The MEMS sensor chip has four rows of 25 sensors with a spanwise separation of $300\ \mu\text{m}$, see figure 1. The length of each hot-film is $150\ \mu\text{m}$ and the width $3\ \mu\text{m}$. It is placed on a $1.2\ \mu\text{m}$ thick silicon-nitride diaphragm with dimensions $200\ \mu\text{m} \times 200\ \mu\text{m}$. Thermal insulation of the hot-film to the substrate is provided by a $2\ \mu\text{m}$ deep vacuum cavity underneath the diaphragm.

The anemometer system (AN1003 from AA lab systems, Israel) has a built-in signal conditioner and the signals from the anemometer were digitized using an A/D converter board (A2000 from National Instruments, USA) in the measurement computer. The A/D converter has 12 bit resolution and four channels which could be sampled simultaneously at rates up to 1 MHz divided by the number of channels used. The complete experiment was run from a program on the measurement computer which controlled the tunnel velocity, the positioning of probes, digitization of the anemometer signals, monitoring of the pressures and the temperature.

3. Experimental procedure

3.1. Hot-wire calibration

The hot-wires were calibrated in the free-stream against the velocity obtained from a Prandtl tube. First, the hot-wire probe was traversed well out of the

boundary layer, then the tunnel was run at ten different velocities ranging from about 5% to 100% of the free-stream velocity and the anemometer's voltage signal and the pressure from the Prandtl tube were recorded. A least-squares fit of the anemometer voltage versus the velocity was formed using Kings law. The calibration procedure was fully automated and the time required was about 15 min. due to the time required to allow the temperature to stabilize after changing the tunnel speed.

3.2. Hot-film calibration

The hot-films were calibrated *in-situ* in the turbulent boundary layer against the mean skin-friction obtained from oil-film interferometry, here denoted τ_w^* .

The principle of oil-film interferometry is to register the temporal deformation of a thin film of oil, due to the shear stress, from the flow, on its upper surface. From the deformation velocity the shear stress can be determined accurately, knowing the viscosity of the oil. The oil-film deformation velocity was determined by measuring the thickness of the oil-film by interferometry, see Fernholz *et al.* (1996). A least-squares fit of a variant of the logarithmic skin-friction law of the type

$$c_f = 2 \left[\frac{1}{\kappa} \ln(Re_\theta) + C \right]^{-2} \quad (1)$$

was made to the obtained wall-shear stress, with the resulting values of the constants $\kappa = 0.384$ and $C = 4.08$, see figure 2. Comparisons with other methods and also other experiments are made in Österlund *et al.* (1999), (see also papers 2 and 4). A detailed description of the method adapted is available in paper 7.

After the mean wall-shear stress relation was determined the anemometer voltage signals, from the two wall-shear stress sensors to be calibrated, were recorded for eight different mean wall-shear stress values in the range $0.3 < \tau_w^* < 3$ times the mean value of interest. This large range was necessary, due to the long tails of the probability density function for τ_w , to avoid extrapolation of the calibration function (2). Kings law was used to relate the anemometer output voltage E to the instantaneous skin-friction τ_w ,

$$\tau_w = \left[\frac{1}{B} (E^2 - A) \right]^{1/n}, \quad (2)$$

where A , B and n are constants. The constants in equation 2 were determined minimizing the sum of the mean-square-error, for all calibration points, between the measured mean skin-friction, τ_w^* , and the mean value, $\overline{\tau_w}$, obtained applying relation 2 to the anemometer voltage signal E :

$$\min \left(\sum (\tau_w^* - \overline{\tau_w})^2 \right). \quad (3)$$

The MEMS hot-film was in Bake & Österlund (1999) (paper 4) found to give

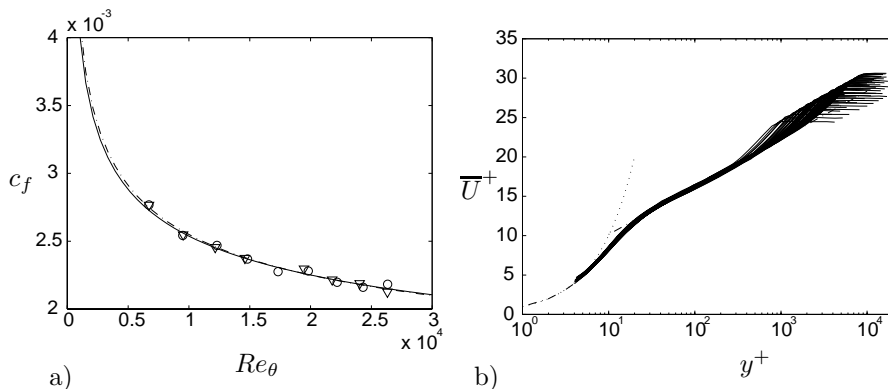


FIGURE 2. Mean flow characteristics of the boundary layer. $2530 < Re_\theta < 27300$. a) Skin-friction coefficient. \circ and ∇ : oil-film interferometry. $---$: best-fit of logarithmic friction law (equation 1) to the oil-film data. $—$: Skin-friction law from Fernholz & Finley (1996). b) Mean velocity profiles shown in inner law scaling of the wall distance. Dashed curves represent $U^+ = y^+$ and $U^+ = \frac{1}{0.38} \ln y^+ + 4.1$

a relative fluctuation intensity of 0.35 (at $Re_\theta \approx 12400$), *i.e.* somewhat lower than the correct value of 0.41 (see Bake & Österlund 1999). This should not be of significant influence for the present correlation measurements.

3.3. Mean Flow Characteristics

Velocity profiles at five different streamwise positions ($x = 1.5, 2.5, \dots, 5.5$ m) were taken over a large span in Reynolds number ($2530 < Re_\theta < 27300$), see figure 2. The behavior of the boundary layer was found to confirm the traditional two layer theory with a logarithmic overlap region for $200\nu/u_\tau < y < 0.15\delta_{95}$ existing for $Re_\theta > 6000$. The values of the von Kármán constant and the additive constants were found to be $\kappa = 0.38$, $B = 4.1$ and $B_1 = 3.6$ ($\delta = \delta_{95}$), see Österlund *et al.* (1999) and paper 2.

3.4. Detection of events

In the detection of shear layer structures the variable-interval time average (VITA) was used. The VITA of a fluctuating quantity $Q(x_i, t)$ is defined by

$$\widehat{Q}(x_i, t, T) = \frac{1}{T} \int_{t-\frac{1}{2}T}^{t+\frac{1}{2}T} Q(s) ds, \quad (4)$$

where T is the averaging time. The conventional time average results when T becomes large, *i.e.*

$$\overline{Q}(x_i) = \lim_{T \rightarrow \infty} \widehat{Q}(x_i, t, T). \quad (5)$$

Blackwelder & Kaplan (1976) used the VITA technique to form a localized measure of the turbulent energy

$$var(x_i, t, T) = \frac{1}{T} \int_{t-\frac{1}{2}T}^{t+\frac{1}{2}T} u^2(s) ds - \left(\frac{1}{T} \int_{t-\frac{1}{2}T}^{t+\frac{1}{2}T} u(s) ds \right)^2. \quad (6)$$

This quantity is also known as the short-time variance of the signal. The VITA variance can be used to detect shear-layer type events. An event is considered to occur when the amplitude of the VITA variance exceeds a certain threshold level. The correspondence between shear-layers and VITA events was substantiated by *e.g.* Johansson & Alfredsson (1982) and Johansson *et al.* (1987*b*). A detection function is defined as

$$D_u(t, T) = \begin{cases} 1 & var > k\overline{u^2} \\ 0 & \text{otherwise} \end{cases}, \quad (7)$$

where k is the detection threshold level. A set of events $E_u = \{t_1, t_2, \dots, t_N\}$ was formed from the midpoints of the peaks in the detection function D_u (N is the total number of detected events). Conditional averages of a quantity Q can then be constructed as

$$\langle Q(\tau) \rangle = \frac{1}{N} \sum_{j=1}^N Q(t_j + \tau), \quad (8)$$

where τ is the time relative to the detection time.

In addition to detecting events using the VITA variance technique, events were detected on the amplitude of the fluctuating quantity itself, *e.g.* detection of peaks of the fluctuating wall-shear stress,

$$D_{\tau_w}(t, T) = \begin{cases} 1 & \tau_w > k\sqrt{\overline{\tau_w^2}} \\ 0 & \text{otherwise} \end{cases}, \quad (9)$$

where k is the threshold level.

4. Results

4.1. Streak spacing

The mean spanwise separation between low-speed streaks in the viscous sub-layer was investigated using the MEMS array of hot-films, see figure 1. This setup allowed for 18 different spanwise separations in the range $0 < \Delta z^+ < 210$. The spanwise length of the hot-films was $l^+ = 5.6$, at the Reynolds number $Re_\theta = 9500$ ($Re_\tau \equiv \delta_{95} u_\tau / \nu = 2300$). The spanwise cross correlation coefficient

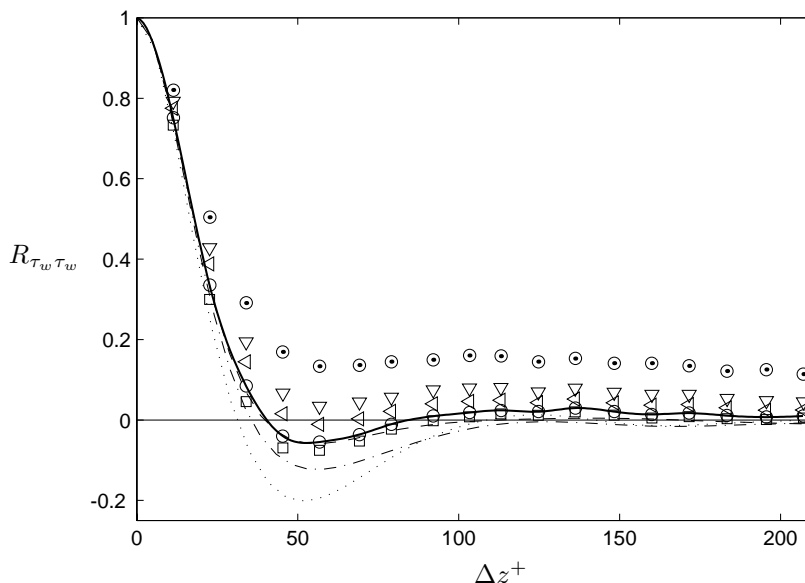


FIGURE 3. Spanwise correlation coefficient $R_{\tau_w \tau_w}$ as a function of Δz^+ , $Re_\theta = 9500$ ($Re_\tau = 2300$). Present data, \odot : unfiltered, ∇ : $f_c^+ = 1.3 \times 10^{-3}$, \triangleleft : $f_c^+ = 2.6 \times 10^{-3}$, \circ : $f_c^+ = 5.3 \times 10^{-3}$, \square : $f_c^+ = 7.9 \times 10^{-3}$, —: spline fit to \circ . DNS of channel flow, correlations of u at $y^+ = 5$, —: $Re_\tau = 590$, - · -: $Re_\tau = 395$, · · ·: $Re_\tau = 180$ (Kim *et al.* 1987; Moser *et al.* 1999).

between the wall-shear stress signals obtained from two hot-films separated a distance Δz^+ in the spanwise direction is defined by

$$R_{\tau_w \tau_w}(\Delta z) = \frac{\overline{\tau_w(z) \tau_w(z + \Delta z)}}{\tau_w'^2}. \quad (10)$$

The prime denotes r.m.s value. The cross-correlation coefficient was used to estimate the mean streak spacing. At high Reynolds numbers contributions to the spanwise correlation coefficient from low frequency structures originating in the outer region conceals the contributions from the streaks and no clear (negative) minimum is visible in figure 3 for the measured correlation coefficient (shown as \odot). This behavior has also been found by others, see *e.g.* Gupta *et al.* (1971). A trend is clearly visible in the relatively low Reynolds number simulations by Kim *et al.* (1987) and Moser *et al.* (1999) where at their highest Reynolds number the minimum is less pronounced. In an attempt to reveal and possibly obtain the streak spacing also from the high Reynolds number data in

the present experiment we applied a high-pass (Chebyshev phase-preserving) digital filter to the wall-shear stress signals before calculating the correlation coefficient. This procedure emphasizes the contribution from the streaks and enhances the variation in the correlation coefficient. A variation of the cut-off frequency revealed no significant dependence of the position of the minimum on the cut-off. The cut-off frequency was chosen to damp out contributions from structures larger than about 2500 viscous length scales, or equivalently, larger than the boundary layer thickness. The filtered correlation is shown for different cut-off frequencies in figure 3. The correlation decreases rapidly and a broad minimum is found at $\Delta z^+ \approx 55$ indicating a mean streak spacing of $\lambda^+ \approx 110$. The correlation coefficient is close to zero for separations $\Delta z^+ > 100$. This result agrees well with other experiments and simulations at low Reynolds numbers, see *e.g.* Kline *et al.* (1967), Kreplin & Eckelmann (1979), Smith & Metzler (1983), Kim *et al.* (1987) and Moser *et al.* (1999). Gupta *et al.* (1971) also used a filtering technique to extract information about streak spacing from two-point correlations. They based their filtering on the VITA technique *i.e.* using short time averages. It is interesting to note that they found that the maximum averaging time for the VITA correlation to give consistent values of the streak spacing was $0.5\delta/U_\infty$. This corresponds well to the present findings regarding high-pass filtering cut-off frequencies.

4.2. Propagation velocities

The wall-normal space-time correlations of the wall-shear stress and the stream-wise velocity were measured using one hot-film sensor and one hot-wire traversed in the (x, y) -plane. The time-shift of the peaks of the correlation coefficient,

$$R_{\tau_w u}(\Delta x, \Delta y, \Delta t) = \frac{\overline{\tau_w(x, y, t)u(x + \Delta x, y + \Delta y, t + \Delta t)}}{\overline{\tau_w' u'}}, \quad (11)$$

for different Δx and Δy separations are shown in figure 4. The peak in the correlation moves to negative time-shifts for increasing wall distances, *i.e.* the structures are seen earlier away from the wall. This indicates a forward leaning structure. The propagation velocity of the structure at different distances from the wall is defined by the slopes

$$C_p^+ = \frac{\Delta x^+}{\Delta t^+} \quad (12)$$

of lines fitted to the time-shifts at constant wall-distance in figure 4. The resulting propagation velocity is plotted in figure 5 and was found to be constant ($C_p^+ \approx 13$) up to about $y^+ = 30$. Further out it was found to be close to the local mean velocity. This means that the structure becomes stretched by the mean shear above $y^+ = 30$. This can be seen also from the variation of the shear layer angle with wall distance, see figure 11.

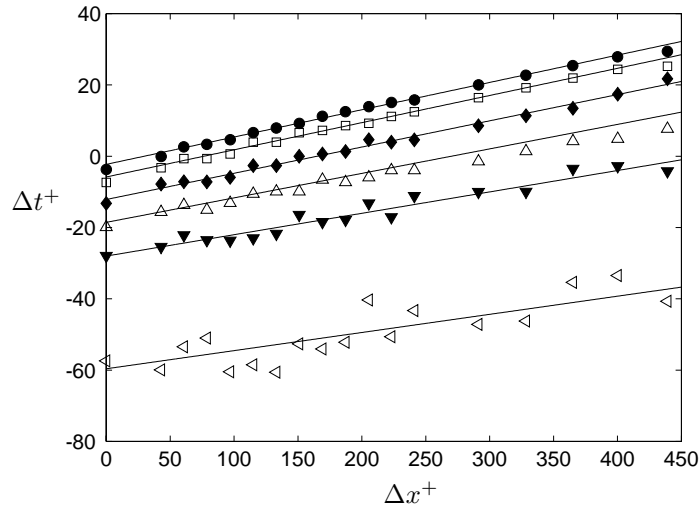


FIGURE 4. Time-shift of maximum correlation, $\max(R_{u\tau_w})$, at different wall distance. \bullet : $y^+ = 5$. \square : $y^+ = 10$. \blacklozenge : $y^+ = 20$. \triangle : $y^+ = 50$. \blacktriangledown : $y^+ = 100$. \triangleleft : $y^+ = 300$.

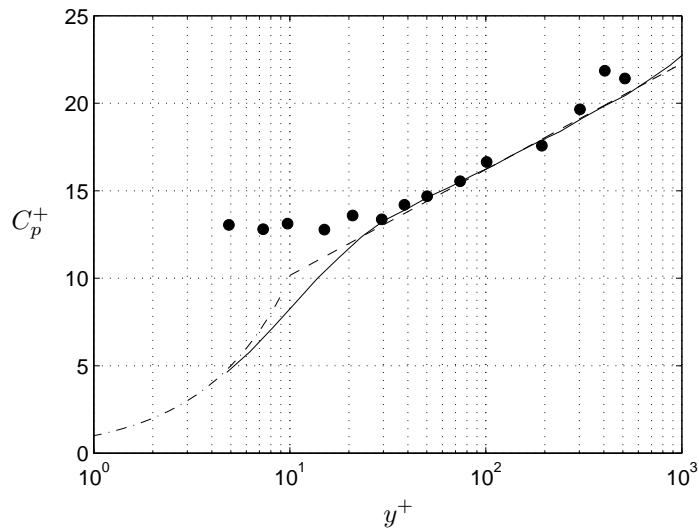


FIGURE 5. Propagation velocity C_p^+ , \bullet . $---$: log-law, $\kappa = 0.38$ and $B = 4.1$. $- \cdot -$: linear profile. $---$: mean velocity profile. $Re_\theta = 9500$.

Symbol	Re_θ	l^+	y^+
\triangle	6700	6.6	14.3
∇	8200	8.2	13.8
*	9700	9.7	14.5
+	12600	12.8	14.8
o	15200	15.8	15.2

TABLE 1. Hot-wire experiments used for VITA detection in the buffer layer.

4.3. Shear-layer events

Shear-layer events were detected from peaks in the short time variance as described in section 3.4 using the velocity signal from a hot-wire in the buffer layer. In table 1 an overview is given of the hot-wire measurements used for VITA detection. An example of the fluctuating velocity signal (top), the corresponding short time variance (center), and the detection function (bottom) are shown in figure 6. The detection times are taken as the midpoints of the peaks of the detection function. The events are further sorted on the derivative of the velocity signal into accelerating and decelerating events, and an ensemble average is formed for each type according to equation 8. The accelerating events dominate in number over the decelerating events, and correspond to a forward leaning shear layer structure. In figure 7 the conditionally averaged streamwise velocity signal in the buffer region ($y^+ \approx 15$) is shown and strong accelerated and decelerated shear-layer events can be clearly seen.

Alfredsson & Johansson (1984) investigated the scaling laws for turbulent channel flows and found that the governing timescale for the near-wall region was a mixture of the inner and outer time scales

$$t_m = \sqrt{t_* t_o}. \quad (13)$$

The frequency of occurrence of the VITA events is shown in figure 8 against the averaging time for outer, mixed and inner scaling. The mixed scaling appears relatively satisfactory also for the boundary layer flow. For very small averaging times one should keep in mind the non-negligible influence of finite probe size for the highest Reynolds numbers, see table 1. Blackwelder & Haritonidis (1983) reported inner scaling for the ‘bursting frequency’ obtained by the VITA technique. However, their values for the friction velocities (obtained from the near-wall linear profile) deviate substantially from the present correlation for c_f and their mean velocity profiles for different Reynolds numbers show a wide spread in the log-region.

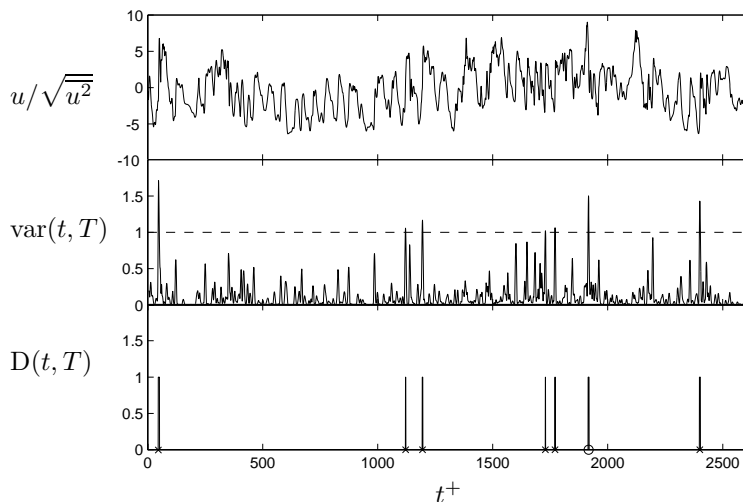


FIGURE 6. a) Time series for the streamwise fluctuating velocity component u . $y^+ = 14.5$ and $Re_\theta = 9700$. b) Short time variance of u with integrating window $T^+ = 10$. c) Detection function for $k = 1.0$. \times : Represents accelerating events and \circ : represents decelerating events.

4.4. Wall-shear stress events

The wall shear stress signal is highly intermittent (flatness factor ≈ 4.9) and peaks in the wall-shear stress was used to detect events. In figure 9 the conditionally averaged wall-shear stress events are shown sorted into positive and negative peaks using different detection threshold levels $k = \{-1, -0.75, -0.5, 1, 2, 3\}$. Broad peaks are seen that are largely symmetric. The negative events are slightly wider and less pointed as compared to the positive events.

Detection on peaks in the wall-shear stress was used to form conditional averages for the streamwise velocity obtained at a wall-normal separation Δy^+ . Conditional averages for the streamwise velocity are shown in figure 10 for different wall-normal separations above the hot-film used as detector. For increasing wall-distance the conditionally averaged velocity is shifted towards negative times indicating a forward leaning structure. In figure 11 the data in figure 10 are replotted into lines of constant disturbance velocity (normalized with the local r.m.s.-level) in the (x, y) -plane using the measured propagation velocities (figure 5) to transform the time to an x -coordinate. An elongated and forward leaning high-velocity structure is visible above the high wall-shear event detected at $x = 0$. The peaks of the conditionally averaged velocity in

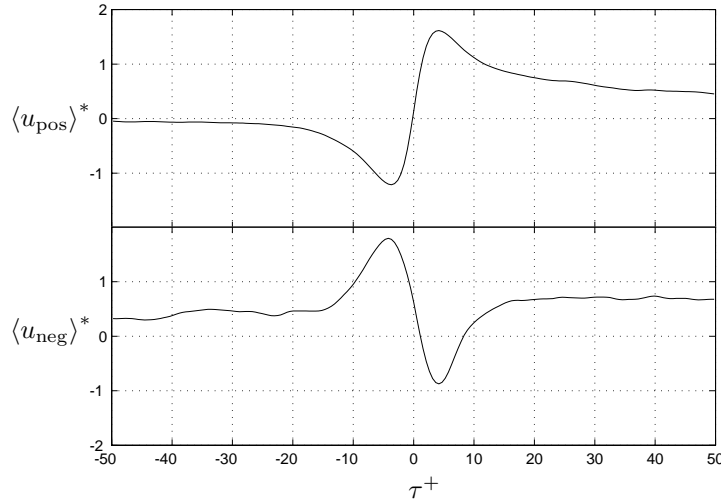


FIGURE 7. Conditional average of u for events with positive slope (top) and negative slope (bottom). $T^+ = 10$, $k = 1.0$ and $Re_\theta = 9700$

figure 10 are shown as black circles and agree well with a shear layer angle of about 20° found in many investigations, see *e.g.* Johansson *et al.* (1987a).

5. Conclusions

A micro machined hot-film sensor array was used together with a hot-wire probe in series of measurements of coherent structures in turbulent boundary layers. The small dimensions of the hot-films was a necessity for these measurements and the spatial resolution satisfactorily high to determine *e.g.* the streak spacing.

A new high-pass correlation technique was used to determine the mean streak spacing for a high Reynolds number turbulent boundary layer. The mean streak spacing was found to be $\lambda^+ \approx 110$ which is very close to previous findings in low Reynolds number flow.

The propagation velocity of disturbances in the boundary layer is constant to $13u_\tau$ up to $y^+ = 30$, further out it was found to be close to the local mean velocity.

It was found that the frequency of occurrence of VITA events in the buffer region approximately conforms, to a mixed scaling behavior.

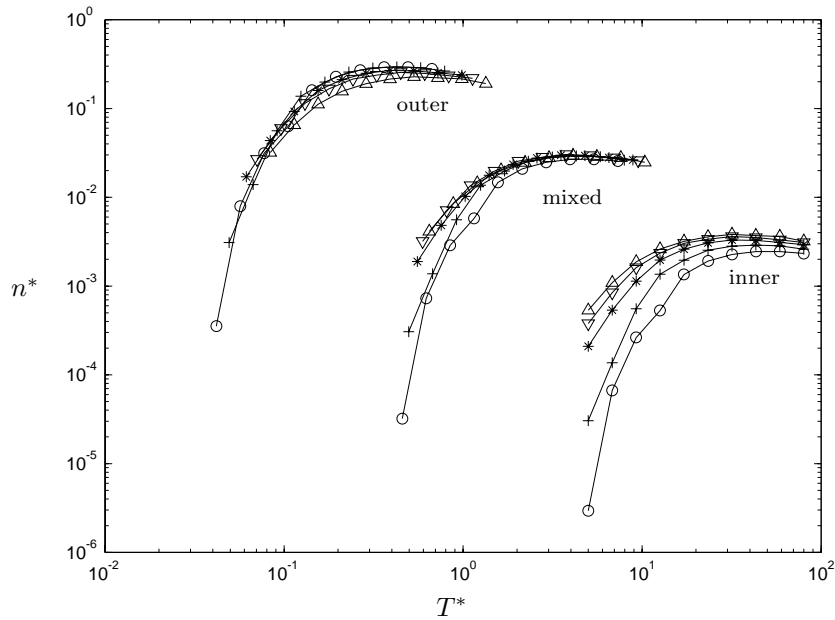


FIGURE 8. Frequency of occurrence of VITA events ($k=1$) as a function of the averaging time with outer, mixed and inner scaling (* denotes nondimensional quantities). $y^+ = 15$, $k = 1.0$. For symbols see table 1.

6. Acknowledgments

The authors wish to thank Professor Chih-Ming Ho at UCLA for providing us with the MEMS hot-film probe. We would like to thank Professor Henrik Alfredsson for many helpful discussions. We also wish to thank Mr. Ulf Landen and Mr. Marcus Gällstedt who helped with the manufacturing of the experimental set-up. Financial support from NUTEK and TFR is gratefully acknowledged.

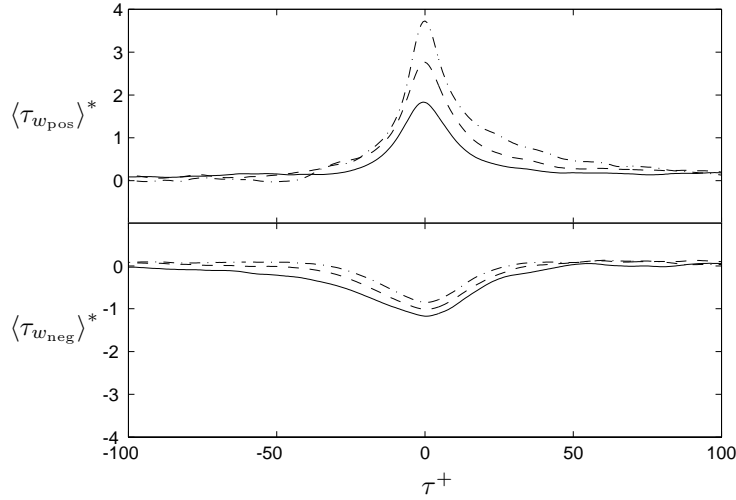


FIGURE 9. Conditional average of τ_w detecting on positive peaks (top) and detecting on negative peaks (bottom). Positive peaks, detection levels, $-\cdot-$: $k = 3$, $--$: $k = 2$, $-$: $k = 1$. Negative peaks, detection levels, $-\cdot-$: $k = -0.5$, $--$: $k = -0.75$, $-$: $k = -1$. $Re_\theta = 9700$.

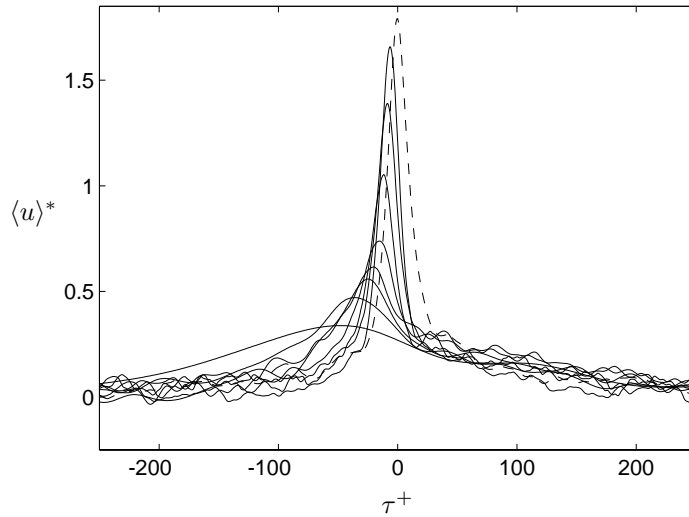


FIGURE 10. Conditionally averaged streamwise velocity. Detection of events where $\tau_w > k\tau_{w,r.m.s.}$. $\Delta x = 0$. $y^+ = \{5.7, 9.6, 16.6, 29.2, 51.7, 92.1, 164, 294\}$. Dashed line is the detection signal $\langle \tau_w \rangle^*$ ($k = 1$).

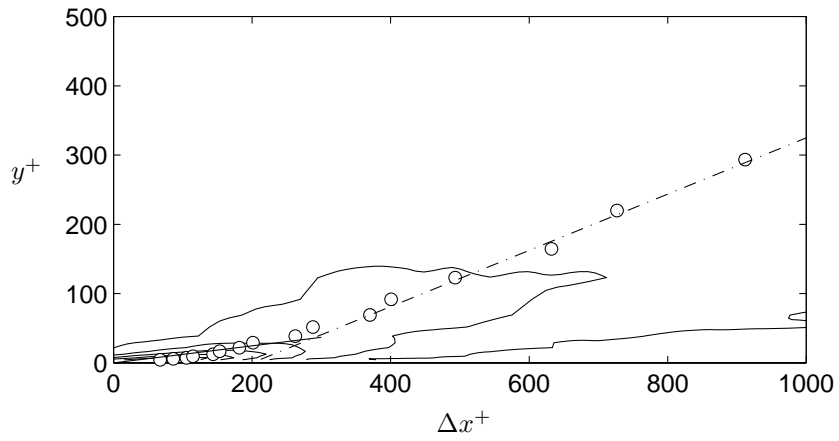


FIGURE 11. Conditionally averaged streamwise velocity. Detection of events where $\tau_w > k\tau_{w,r.m.s.}$. $k = 1$. \circ : locations of maximum correlation. —: slope 7° . - · -: slope 18° .

References

- ALFREDSSON, P. H. & JOHANSSON 1984 Time scales in turbulent channel flow. *Phys. Fluids A* **27** (8), 1974–81.
- BAKE, S. & ÖSTERLUND, J. M. 1999 Measurements of skin-friction fluctuations in turbulent boundary layers with miniaturized wall-hot-wires and hot-films. Submitted for publication in *Phys. of Fluids*.
- BLACKWELDER, R. F. & HARITONIDIS, J. H. 1983 The bursting frequency in turbulent boundary layers. *J. Fluid Mech.* **132**, 87–103.
- BLACKWELDER, R. F. & KAPLAN, R. E. 1976 On the wall structure of the turbulent boundary layer. *J. Fluid Mech.* **76**, 89–112.
- CHEN, K. K. & BLACKWELDER, R. F. 1978 Large-scale motion in a turbulent boundary layer. *J. Fluid Mech.* **89**, 1–31.
- CORINO, E. R. & BRODKEY, R. S. 1969 A visual investigation of the wall region turbulent flow. *J. Fluid Mech.* **37**, 1–30.
- FERNHOLZ, H. H. & FINLEY, P. J. 1996 The incompressible zero-pressure-gradient turbulent boundary layer: An assessment of the data. *Prog. Aerospace Sci.* **32**, 245–311.
- FERNHOLZ, H. H., JANKE, G., SCHÖBER, M., WAGNER, P. M. & WARNACK, D. 1996 New developments and applications of skin-friction measuring techniques. *Meas. Sci. Technol.* **7**, 1396–1409.
- FIEDLER, H. E. 1986 Coherent structures. In *Advances in turbulence*, , vol. 32, pp. 320–336. Berlin: Springer-Verlag.
- GUPTA, A. K., LAUFER, J. & KAPLAN, R. E. 1971 Spatial structure in the viscous sublayer. *J. Fluid Mech.* **50**, 493–512.
- HEAD, M. R. & BANDYOPADHYAY, P. 1981 New aspects of turbulent boundary layer structure. *J. Fluid Mech.* **107**, 297–338.
- HO, C.-M. & TAI, Y.-C. 1998 Micro-electro-mechanical-systems (MEMS) and fluid flows. *Ann. Rev. Fluid Mech.* **30**, 579–612.
- HUSSAIN, A. K. M. F. 1986 Coherent structures and turbulence. *J. Fluid Mech.* **173**, 303–56.
- JIANG, F., TAI, Y.-C., GUPTA, B., GOODMAN, R., TUNG, S., HUANG, J. B. & HO, C.-M. 1996 A surface-micromachined shear stress imager. In *1996 IEEE Micro Electro Mechanical Systems Workshop (MEMS '96)*, pp. 110–115.

- JIANG, F., TAI, Y.-C., WALSH, K., TSAO, T., LEE, G. B. & HO, C.-H. 1997 A flexible mems technology and its first application to shear stress sensor skin. In *1997 IEEE Micro Electro Mechanical Systems Workshop (MEMS '97)*, pp. 465–470.
- JOHANSSON, A. V. 1992 A low speed wind-tunnel with extreme flow quality - design and tests. In *Prog. ICAS congress 1992*, pp. 1603–1611. ICAS-92-3.8.1.
- JOHANSSON, A. V. & ALFREDSSON, P. H. 1982 On the structure of turbulent channel flow. *J. Fluid Mech.* **122**, 295–314.
- JOHANSSON, A. V., ALFREDSSON, P. H. & ECKELMANN, H. 1987a On the evolution of shear layer structures in near wall turbulence. In *Advances in Turbulence* (ed. G. Compte-Bellot & J. Mathieu), pp. 383–390. Springer-Verlag.
- JOHANSSON, A. V., ALFREDSSON, P. H. & KIM, J. 1991 Evolution and dynamics of shear-layer structures in near-wall turbulence. *J. Fluid Mech.* **224**, 579–599.
- JOHANSSON, A. V., HER, J.-Y. & HARITONIDIS, J. H. 1987b On the generation of high-amplitude wall-pressure peaks in turbulent boundary layers and spots. *J. Fluid Mech.* **175**, 119–142.
- KIM, H. T., KLINE, S. J. & REYNOLDS, W. C. 1971 The production of turbulence near a smooth wall in a turbulent boundary layer. *J. Fluid Mech.* **50**, 133–160.
- KIM, J., MOIN, P. & MOSER, R. 1987 Turbulence statistics in fully developed channel flow. *J. Fluid Mech.* **177**, 133–166.
- KLINE, S. J., REYNOLDS, W. C., SCHRAUB, F. A. & RUNSTADLER, P. W. 1967 The structure of turbulent boundary layers. *J. Fluid Mech.* **30**, 741.
- KOVASZNAVY, L. G., KIBENS, V. & BLACKWELDER, R. S. 1970 Large-scale motion in the intermittent region of a turbulent boundary layer. *J. Fluid Mech.* **41**, 283–325.
- KREPLIN, H.-P. & ECKELMANN, H. 1979 Propagation of perturbations in the viscous sublayer and adjacent wall region. *J. Fluid Mech.* **95**, 305–322.
- MOSER, R. D., KIM, J. & MANSOUR, N. N. 1999 Direct numerical simulation of turbulent channel flow up to $Re_\theta = 590$. *Phys. Fluids* **11** (4), 943–945.
- ÖSTERLUND, J. M., JOHANSSON, A. V., NAGIB, H. M. & HITES, M. H. 1999 Wall shear stress measurements in high reynolds number boundary layers from two facilities. In *30th AIAA Fluid Dynamics Conference, Norfolk, VA*. AIAA paper 99-3814.
- RAO, K. N., NARASIMA, R. & BADRI NARAYANAN, M. 1971 The "bursting" phenomenon in a turbulent boundary layer. *J. Fluid Mech.* **48**, 339–352.
- ROBINSON, S. K. 1991 Coherent motions in the turbulent boundary layer. *Ann. Rev. Fluid Mech.* **23**, 601–639.
- SMITH, C. R. & METZLER, S. P. 1983 The characteristics of low-speed streaks in the near-wall region of a turbulent boundary layer. *J. Fluid Mech.* **129**, 27–54.
- WALLACE, J. M., ECKELMANN, H. & BRODKEY, R. 1972 The wall region in turbulent shear flow. *J. Fluid Mech.* **54**, 39–48.
- WILLMART, W. W. & LU, S. S. 1972 Structure of the Reynolds stress near the wall. *J. Fluid Mech.* **55**, 65–92.

